GA–C24119

COMPARISON OF SENSORS FOR RESISTIVE WALL MODE FEEDBACK CONTROL

Milestone #145 "Containing Plasma Instabilities with Metal Walls"

by
E.J. STRAIT, M.S. CHU, A.M. GAROFALO, R.J. LA HAYE,
M. OKABAYASHI, H. REIMERDES, J.T. SCOVILLE, and A.D. TURNBULL

Prepared under
Contract No. DE-AC03-99ER54463
for the U.S. Department of Energy

DATE PUBLISHED: SEPTEMBER 2002

DISCLAIMER

GA–C24119

COMPARISON OF SENSORS FOR RESISTIVE WALL MODE FEEDBACK CONTROL

Milestone #145 "Containing Plasma Instabilities with Metal Walls"

E.J. STRAIT, M.S. CHU, A.M. GAROFALO,† R.J. LA HAYE,
M. OKABAYASHI,‡ H. REIMERDES,† J.T. SCOVILLE, and A.D. TURNBULL

†Columbia University
‡Princeton Plasma Physics Laboratory

Prepared under
Contract No. DE-AC03-99ER54463
for the U.S. Department of Energy

GENERAL ATOMICS PROJECT 30033
DATE PUBLISHED: SEPTEMBER 2002

COMPARISON OF SENSORS FOR RESISTIVE WALL MODE FEEDBACK CONTROL

Report on Milestone 145:
("Containing plasma instabilities with metal walls")

by
E.J. Strait, M.S. Chu, A.M. Garofalo, R.J. La Haye, M. Okabayashi, H. Reimerdes, J.T. Scoville, and A.D. Turnbull

The most serious instabilities in the tokamak are those described by ideal magneto-hydrodynamic theory. These modes limit the stable operating space of the tokamak. The ideal MHD calculations predict the stable operating space of the tokamak may be approximately doubled when a perfectly conducting metal wall is placed near the plasma boundary, compared to the case with no wall (free boundary). The unstable mode distortions of the plasma column cannot bulge out through a perfectly conducting wall. However, real walls have finite conductivity and when plasmas are operated in the regime between the free boundary stability limit and the perfectly conducting wall limit, the unstable mode encountered in that case "the resistive wall mode," can leak out through the metal wall, allowing the mode to keep slowly growing. The slow growth affords the possibility of feedback stabilizing this mode with external coils. DIII-D is making good progress in such feedback stabilization research and in 2002 will use an improved set of mode sensors inside the vacuum vessel and closer to the plasma surface which are expected theoretically to improve the ability to stabilize the resistive wall mode.

1. INTRODUCTION

The external kink instability is a potential obstacle to the achievement of high beta, high bootstrap fraction, steady state tokamak plasmas. Discharges with a large fraction of bootstrap current necessarily have a broad current density profile, and therefore tend to have a low beta limit for the n=1 kink mode. With a conducting wall surrounding the plasma, the beta limit becomes significantly larger. However, a real, resistive wall does not provide complete stability but converts the kink mode to a slowly growing resistive wall mode (RWM). The slow growth rate admits the possibility of stabilizing the mode with feedback control, using non-axisymmetric coils inside or outside the wall.

Theory and DIII–D experiments [1] show that strong plasma rotation can also provide stability above the no-wall beta limit. However, this approach may not be feasible in a burning plasma which has little or no torque from neutral beam heating. Therefore it is important to validate the physics of feedback stabilization of the resistive wall mode.

In this report we summarize predictions and experimental results regarding the use of internal sensors for RWM feedback control in DIII–D. Feedback control of the resistive wall mode in DIII–D is performed with the C-coil, a six-segment set of external coils around the midplane of the tokamak [Fig. 1(a)]. These coils were originally installed for error field correction. With the addition of fast switching amplifiers, the coils are now used for simultaneous error correction and feedback stabilization. Several arrays of resistive wall mode diagnostics are available at the midplane [Fig. 1(b)] and have been used as input for the feedback system. Additional arrays above and below the midplane are used to measure the poloidal mode structure of the RWM. The arrays of radial field sensors (saddle loops) outside the vacuum vessel have been in use since 1998. Based on theoretical predictions of improved performance, new arrays of radial field sensors and poloidal field sensors (magnetic probes) were installed on the inner surface of the vessel for use in 2001.

Section 2 of this report summarizes the numerical modeling predictions that internal sensors are superior to external sensors, and that internal poloidal field sensors are superior to internal radial field sensors, for resistive wall mode feedback control. Section 3 discusses a simple analytic model that supports this prediction and provides some insight into the reasons for the differences between sensors. DIII–D experimental results that confirm these predictions are described in Section 4. Feedback controlled suppression of "resonant field amplification" in stable plasmas is discussed briefly in Section 5.

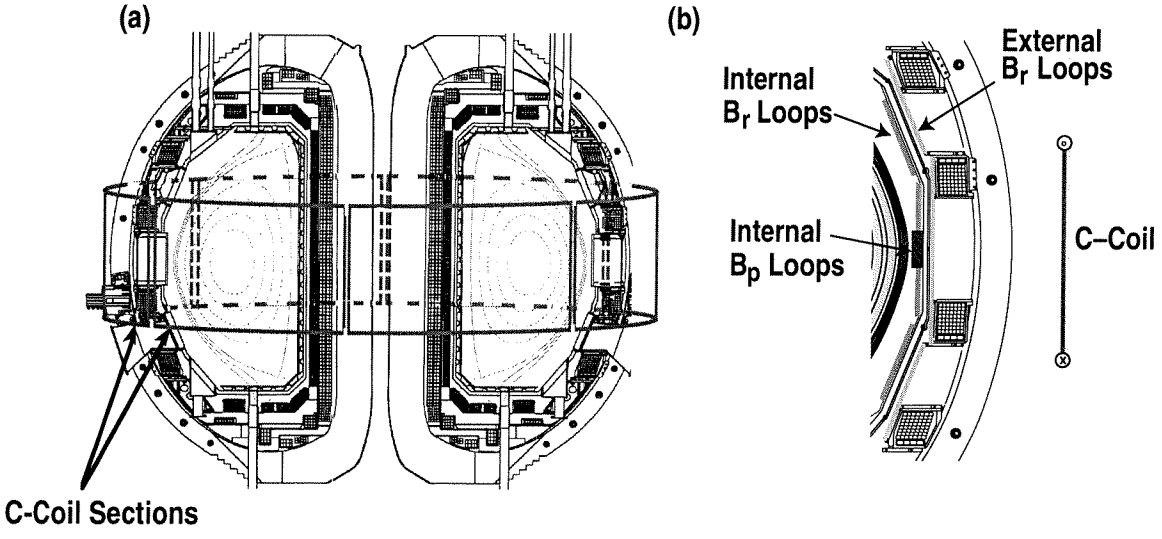

Fig. 1. (a) The 6-segment control coil (C-coil) surrounds the midplane of the DIII–D vacuum vessel. Normally the coils are connected in three opposing (odd toroidal mode number) pairs. (b) Cross-section of the large major radius side of the DIII–D vessel and coils, showing the C-coil, external and internal saddle loops (B_r) and internal magnetic probes (B_p).

2. NUMERICAL FEEDBACK MODELS

The advantages of internal radial field sensors over external sensors originate primarily in their distance from the plasma. Modeling with the MARS code has shown that the feedback performance with radial field sensors is very sensitive to the position of the sensors [2]. In modeling of a JET-like advanced tokamak equilibrium with beta about 1.6 times the no-wall stability limit, the critical gain for stabilization varied by more than a factor of 2 as the radial position of the sensors was increased by about 15% of the plasma's minor radius. This is a result of the increased coupling to the control coils and reduced coupling to the plasma as the sensor radius increases, and provides motivation for placing the sensors inside the wall to reduce the distance from the plasma.

MARS modeling has also predicted superior feedback performance with poloidal field sensors as compared with radial field sensors[2,3]. In modeling of the same JET-like equilibrium, feedback control with poloidal field sensors was found to be more robust than with radial field sensors. Specifically, with poloidal field sensors, the control was much less sensitive to the poloidal width of the control coils and to the radial position of the sensors between the wall and the plasma. The poloidal field sensors were also found to require a dimensionless gain value for the feedback control about half that for radial field sensors in the optimal configuration for each. These results have been further analyzed in terms of control theory [4–6], and are attributed to the vanishing of the mutual inductance between the control coils and poloidal field sensors.

Similar results are obtained from VALEN modeling. The VALEN code [7] uses a detailed, finite-element circuit representation for the plasma mode, resistive wall, and control coils, and can model arbitrary sensor and coil configurations. In the specific geometry of the DIII–D vacuum vessel, midplane control coils, and sensors, poloidal field sensors were again found to have superior performance. As shown in Fig. 2, using the existing external control coils, external radial field sensors were predicted to extend the beta limit by about 20% of the difference between the no-wall limit and the ideal-wall limit. Internal radial field sensors give a modest improvement, to about 30% of the difference between the no-wall limit and the ideal-wall limit, while a 50% extension was predicted with poloidal field sensors.

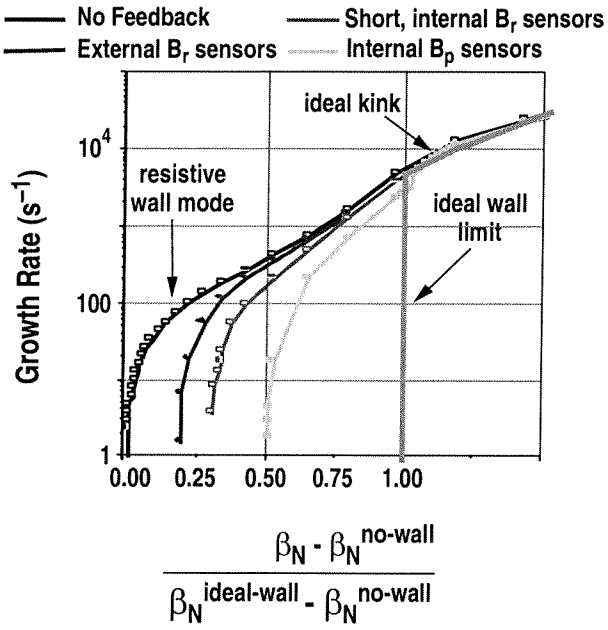

Fig. 2. VALEN predictions for kink mode stabilization in DIII–D, with feedback control using the C-coil set. Shown are cases with no feedback, external radial field sensors, internal radial field sensors, poloidal field sensors, and an ideally conducting wall.

3. ANALYTIC FEEDBACK MODEL

Although less realistic than the numerical models, analytic models with lumped parameters [8–10] can provide valuable insight into the differences between types of sensors. These models can be reduced to a simple set of equations:

$$s - \gamma_0 + G(s)\,F(s) = 0 \quad , \tag{1}$$

$$\Phi = \Phi_P + \Phi_{PW} + \Phi_C + \Phi_{CW} \quad , \tag{2}$$

$$\Phi_P = (1+\gamma_0)\,\Phi \quad , \tag{3}$$

$$\Phi_C = -G(s)\,\Phi_S \quad , \tag{4}$$

$$\Phi_{PW,\,CW} = -\Phi_{P,C}\; s/(1+s) \quad , \tag{5}$$

where in Laplace transform notation $s = \gamma + i\omega$ represents the growth rate and real frequency of the resistive wall mode, and γ_0 is the growth rate in the absence of feedback. The limit where the plasma would be marginally stable with an ideal wall corresponds to $\gamma_0 = \infty$, since this model neglects the plasma's inertia. The dispersion relation [Eq. (1)] is to be solved for the growth rate of the instability. The total perturbed radial flux Φ at the resistive wall includes terms for the flux Φ_P produced by the plasma, the flux Φ_C produced by the control coils, and fluxes Φ_{PW} and Φ_{CW} from wall currents induced by the plasma and control coils respectively [Eq. (2)]. The plasma model [Eq. (3)] relates the plasma perturbation to the perturbed boundary condition at the wall [9]. The transfer function F(s) for the sensors relates the flux Φ_S measured by the sensors to the total perturbed flux Φ, and will be defined below. The feedback gain G(s) then relates the flux Φ_C produced by the control coils to the sensor measurement Φ_S [Eq. (4)]. The fluxes from wall currents [Eq. (5)] are driven by the rate of change of the plasma and control coil fluxes, and oppose the fluxes that drive them. Here the growth rates and frequencies are expressed in units of the wall time constant ($s\tau_{Wall} \rightarrow s$). All of the perturbed fluxes, including the sensor measurements, are evaluated at the wall. The key physics is contained in the model for the unstable plasma, the gain G (which includes the characteristics of the amplifier-control coil system, and may be frequency dependent), and the sensor's transfer function F. For this discussion we will assume an idealized amplifier-coil system, with a constant proportional gain at all frequencies.

The different types of sensors can be characterized by their response to the different parts of the perturbed flux:

Idealized Mode Detection $\Phi_S = \Phi_P$, (6)

Smart Shell $\Phi_S = \Phi_P + \Phi_{PW} + \Phi_C + \Phi_{CW}$, (7)

DC Compensated B_r Sensor $\Phi_S = \Phi_P + \Phi_{PW} + \Phi_{CW}$, (8)

AC Compensated B_r Sensor $\Phi_S = \Phi_P + \Phi_{PW}$, (9)

B_p Sensor $\Phi_S = \Phi_P - \Phi_{PW}$. (10)

An idealized sensor [Eq. (6)] would detect the plasma perturbation and nothing else. In the "Smart Shell" control scheme [Eq. (7)] the sensor simply detects the total perturbed radial flux at the wall, with the aim of controlling it to be zero in order to mimic the response of a perfectly conducting wall. Note that the response of a radial field sensor is the same whether it is located on the inner or outer surface of the wall. The control coil currents and their coupling to the sensors are well characterized, and their direct effects can be subtracted from the sensor signal ([Eq. (8)]. The wall response to the control coils is also predictable and can be subtracted from the sensor signal [Eq. (9)]. In DIII–D, because of the symmetry of the sensors and coils at the midplane, the poloidal field sensors are naturally decoupled from the control coils and their induced wall currents, and respond only to the plasma perturbation and the wall current that it induces [Eq. (10)]. In Eq. (10), the poloidal field sensor has been defined in terms of the perturbed *radial* flux, with an implicit 90° phase shift from the actual measured poloidal field, so that the form of the model in Eqs. (1–5) can be maintained. For poloidal field sensors inside the wall, the field from the wall current reinforces the field from the plasma perturbation, a key difference from the AC compensated radial field sensor. This change in sign of the wall response for poloidal field sensors is expressed by changing the sign of Φ_{PW} in Eq. (10), so that Eq. (15) keeps the same form for all cases.

Each of the sensor definitions [Eqs. (6–10)] can be substituted into the model of Eqs. (1–5). The dispersion relation then yields the following conditions for stability ($\gamma < 0$):

Idealized Mode Detection $G > \gamma_0/(1+\gamma_0)$, (11)

Smart Shell B_r Sensor $G > \gamma_0$, (12)

DC Compensated B_r Sensor $G > \gamma_0/(1+\gamma_0)$ and $G < 1$, (13)

AC Compensated B_r Sensor $\quad G > \gamma_0/(1+\gamma_0)$ and $\gamma_0 < 1$, (14)

B_p Sensor $\quad G > \gamma_0/(1+\gamma_0)$. (15)

With an idealized sensor [Eq. (11)] a feedback system *with finite gain* can reproduce the stabilizing effect of an ideal wall; that is, a mode with an arbitrarily large growth rate γ_0 can be stabilized by a finite gain ($G \geq 1$). With "Smart Shell" control [Eq. (12)], a mode with any finite growth rate can be stabilized, but the minimum required gain becomes large as the mode growth rate increases. With DC compensated radial field sensors [Eq. (13)], a mode with an arbitrarily large growth rate can be stabilized by a finite gain. However, the gain must also remain less than unity, meaning that the range of stable gain values becomes very narrow as γ_0 increases. With AC compensated radial field sensors [Eq. (14)], only modes having low growth rates ($\gamma_0 < 1$) can be stabilized. On the other hand, the poloidal field sensor [Eq. (15)] recovers the same stability condition as the idealized sensor. These results are summarized in Fig. 3.

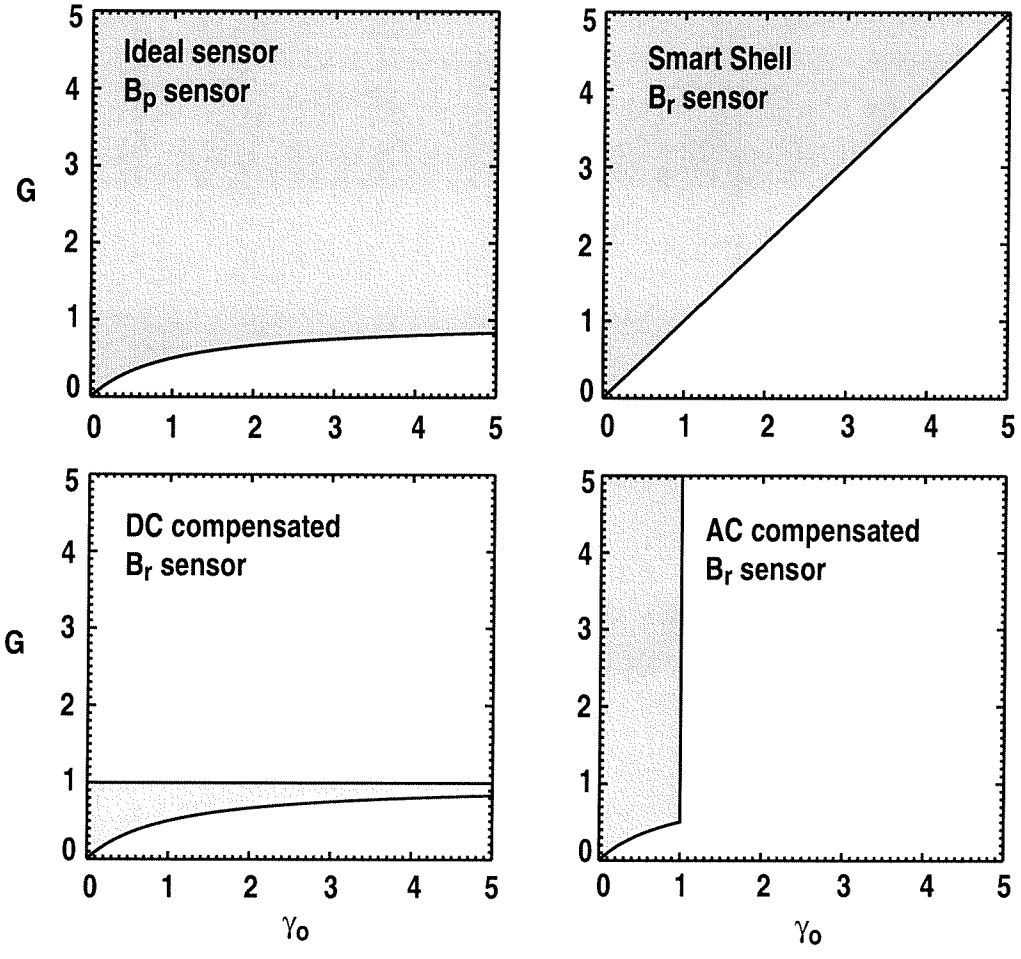

Fig. 3. Range of gain values G (shaded) to stabilize a mode with open-loop growth rate γ_0, for various types of sensors located just inside the resistive wall.

This simple model suggests that poloidal field sensors can realize the same performance as an ideal mode amplitude sensor, allowing stabilization up to the ideal-wall limit with a modest feedback gain G~1. The schemes considered using radial field sensors all have significant drawbacks: a very large gain requirement, a very narrow range of stable gain values, or the capability only to control weakly unstable modes.

The reasons for the difference in performance can be understood by combining the sensor definitions [Eqs. (6–10)] with Eqs. (2), (3) and (5) to express the relationship of each type of sensor signal to the plasma perturbation:

Idealized Mode Detection	$\Phi_S = \Phi_P$	(16)
Smart Shell	$\Phi_S = \Phi_P /(1+\gamma_0)$	(17)
DC Compensated B_r Sensor	$\Phi_S = \Phi_P [1-s/(1+\gamma_0)]$	(18)
AC Compensated B_r Sensor	$\Phi_S = \Phi_P/(1+s)$	(19)
B_p Sensor	$\Phi_S = \Phi_P [1+ s/(1+s)]$	(20)

The smart shell sensor signal [Eq. (17)] decreases as the mode growth rate γ_0 increases, requiring larger gain to be used. The DC compensated signal [Eq. (18)] has a time derivative (~s) term with a destabilizing sign. The AC compensated signal [Eq. (19)] is a low-pass filtered version of the idealized sensor signal, with a bandwidth of 1. Thus it should not be expected to perform well for growth rates of $\gamma_0>1$, even though it is decoupled from the control coils. The B_p sensor [Eq. (20)] is equivalent to the idealized sensor, plus an additional high-pass filtered term that *improves* the sensitivity at high frequencies. Thus, one important conclusion is that a key advantage of poloidal field sensors over radial field sensors is their faster time response, not simply their decoupling from the control coils as is often stated.

The model also predicts a strong sensitivity to the location of radial field sensors, as did the numerical models. As shown above, with smart shell B_r sensors at the wall, a mode with an arbitrarily large growth rate can be stabilized but the required gain becomes large as the mode growth rate increases. If the sensor is moved from the wall toward larger radius, the coupling to the control coil increases relative to the other contributions in the measured flux. As a result, there appears a finite upper limit to the growth rate that can be stabilized, even in the limit of very large gain. On the other hand, if the sensor is moved from the wall toward smaller radius, closer to the plasma, then it becomes possible to stabilize an arbitrarily large growth rate with a finite gain, similar to the idealized and poloidal field sensors. (However, this finite gain may be

quite large if the B_r sensor is not far from the wall.) A poloidal field sensor inside the wall is much less sensitive to position.

In more realistic modeling there may be additional restrictions on the performance of the feedback system, including the finite bandwidth of the amplifier-coil system. However, the inclusion of a single-pole high frequency cutoff at a frequency ω_0 does not lead to qualitative changes in the results. The conditions (11–15) on the gain values remain the same. The idealized sensor, smart shell, and poloidal field sensor schemes require the bandwidth to be greater than the natural growth rate of the mode: $\omega_0 > \gamma_0$, while the "mode control" schemes with compensated radial field sensors require even larger bandwidths.

4. DIII–D EXPERIMENTAL RESULTS

DIII–D experimental results are consistent with the modeling predictions that internal radial field sensors perform better than external radial field sensors for resistive wall mode feedback control, and that poloidal field sensors give still better performance. In the experiments described here, the discharge is programmed with a plasma current ramp of 1.6 MA/s during the high power heating phase. The rapid current ramp maintains a broad current density profile with low internal inductance, which has a low kink mode beta limit without a conducting wall but a significantly higher beta limit with a conducting wall. In the presence of the real, resistive wall, these plasmas are subject to strong resistive wall mode instabilities that cause an early beta collapse.

Internal radial field sensors (saddle loops) are found to yield a modest improvement in feedback control over the external saddle loops, as shown in Fig. 4. In this comparison [11,12], "smart shell" control using the external saddle loops extended the duration of the high beta phase of the discharge by about 50 ms, while use of the internal saddle loops extended the duration by an additional 50 ms. This is consistent with the predictions of the analytic models and the more detailed predictions of MARS and VALEN (Fig. 2) that there is a modest improvement from moving the radial field sensors closer to the plasma.

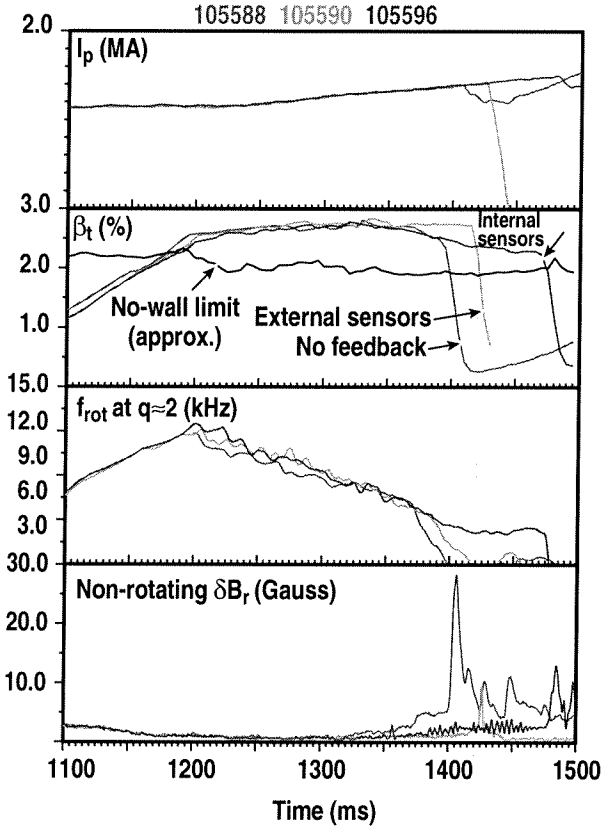

Fig. 4. Comparison of feedback control with internal and external radial field sensors, and no feedback, showing the time evolution of (a) plasma current, (b) normalized beta, (c) toroidal rotation at the q=2 surface, and (d) amplitude of the n=1 resistive wall mode.

Poloidal field sensors yield a greater improvement of RWM stability. In the discharges shown in Fig. 5, feedback using the internal saddle loops extended the high beta duration by only about 40 ms over the case with no feedback. In comparison, the use of poloidal field sensors not only extended the duration by up to 200 ms over the no-feedback case, but also allowed the discharge to reach higher beta. With poloidal field sensors, the beta here reaches a value about 50% higher than the estimated no-wall stability limit. It is well known that plasma rotation is an important stabilizing influence on the RWM. However, in this experiment,

designed to have a strongly unstable RWM, there are at least two indications that active feedback is necessary for the plasma to remain stable. First, note that the cases in Fig. 5 without feedback and with radial field feedback experience the beta collapse only after a relatively slow decay of the plasma rotation. On the other hand, there is no preliminary decay of the rotation in the cases with poloidal field feedback; that is, loss of rotation is not the reason the plasma becomes unstable. Second, in some of these discharges the feedback control was turned off for brief intervals, leaving the control-coil current constant. In the example shown in Fig. 6, the feedback is first switched off from 1350 to 1360 ms. There is no indication of an instability, as expected since the case without feedback was stable at this time. The feedback is again switched off from 1450 to 1460 ms, which is after the time when the cases without feedback and with radial field feedback became unstable. A resistive wall mode grows, reaches an amplitude of about 3 G, and then decays when the feedback is restored. A small decrease in beta also occurs during the instability. This clearly shows that feedback control is necessary for stability of the plasma.

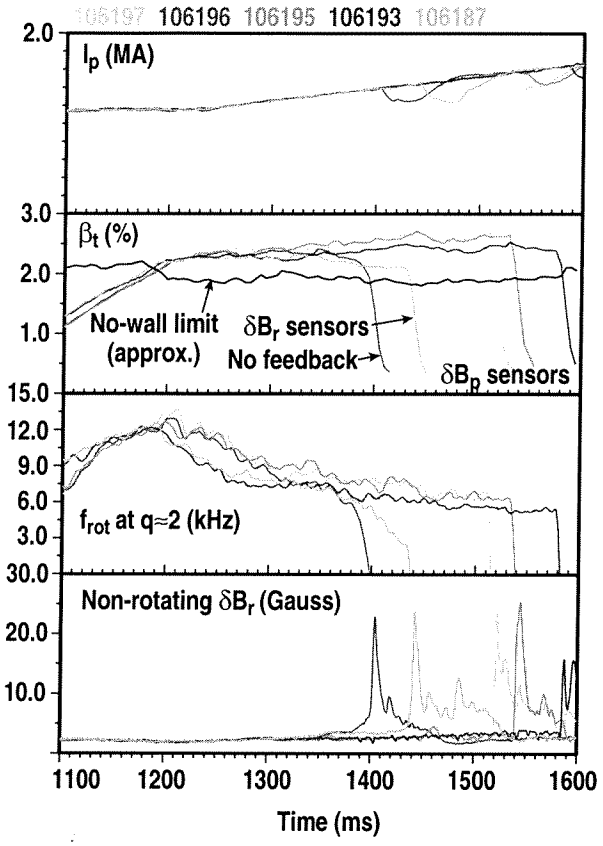

Fig. 5. Comparison of feedback control with poloidal field sensors, radial field sensors, and no feedback, showing the time evolution of (a) plasma current, (b) normalized beta, (c) toroidal rotation at the q=2 surface, and (d) amplitude of the n=1 resistive wall mode.

Direct measurements of the RWM growth rate show that feedback control with poloidal field sensors stabilizes more strongly unstable resistive wall modes, as predicted by the analytic models. When the RWM becomes unstable, the control coil currents saturate early in the growth of the mode and can no longer follow the command of the feedback system. Therefore, the observed growth rate during the beta collapse should be a good approximation of the no-feedback growth rate. This observed growth rate is plotted in Fig. 7 for a set of discharges that includes those of Fig. 6. The abcissa is β_N/ℓ_i; discharges of the type used here with a fast current ramp have been found empirically and from GATO stability calculations to have a no-wall stability limit of $\beta_N/\ell_i \sim 2.4$. As expected, the RWM growth rate in Fig. 7 increases rapidly as beta is raised above the no-wall stability limit. Without feedback the RWM has a growth rate of $\gamma\tau_{wall} \sim 1$ as expected. Radial field sensors provide stability up to $\gamma\tau_{wall} \sim 2$, with little

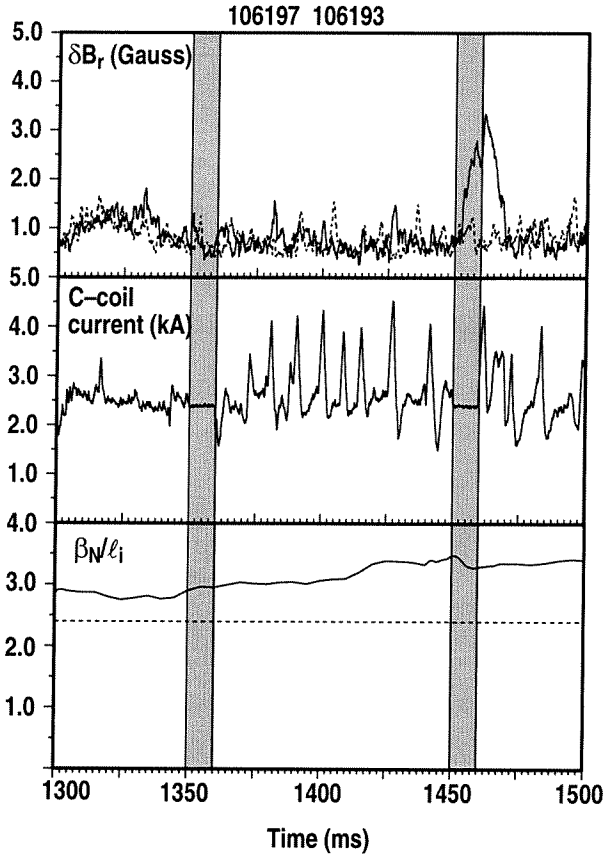

Fig. 6. Effects of switching off the feedback control (shaded intervals) in discharge 106197, showing (a) RWM amplitude from the radial field sensors, (b) current in one of the C-coil pairs, and (c) the stability parameter β_N/ℓ_i

improvement in beta. However, poloidal field sensors provide stability up to $\gamma\tau_{wall} \sim 6$, with an improvement in the stability limit up to $\beta_N/\ell_i \sim 3.3$.

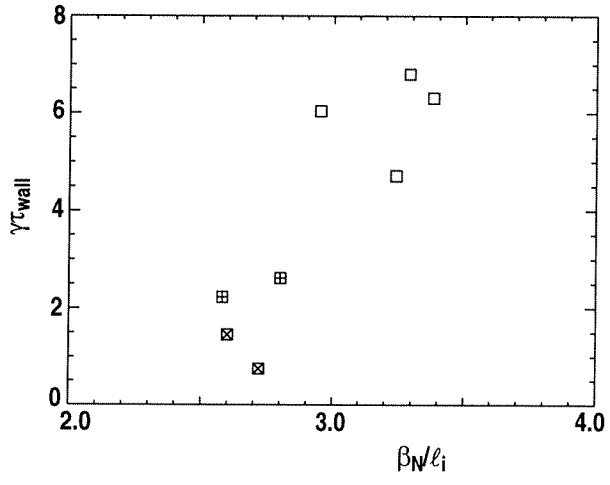

Fig. 6. Observed resistive wall mode growth rate, normalized to the wall time constant $\tau_{wall} \sim 5$ ms, versus the stability parameter β_N/ℓ_i. Shown are cases with no feedback (x), radial field feedback (+), and poloidal field feedback with varying amounts of derivative gain (❑).

5. FEEDBACK CONTROL OF RESONANT FIELD AMPLIFICATION

Recent research has shown that the resonant response of a stable RWM to a static, external n=1 field can be an important effect that causes strong damping of the plasma rotation as the plasma approaches marginal stability [13]. DIII–D experiments [1,10] have shown that feedback control can be an effective tool in reducing this "Resonant Field Amplification," thus allowing the plasma to maintain a high rotational frequency that stabilizes the RWM.

DIII–D experiments have consistently shown that feedback control to suppress resonant field amplification is much more effective with poloidal field sensors than with radial field sensors. In this case, the important factor is the decoupling of the poloidal field sensors from the control coils. Resonant field amplification is a quasi-DC process, so the time response of the sensors is not important. The difference in the sensors can be easily understood by considering a perfect feedback system (i.e., the limit of large gain). The model of Eqs. (1–5) now becomes

$$\Phi_S = 0 \quad , \tag{21}$$

$$\Phi = \Phi_P + \Phi_C + \Phi_0 \quad , \tag{22}$$

$$\Phi_P = (1+\gamma_0)\,\Phi \quad . \tag{23}$$

A perfect feedback system regulates the sensor signal to zero [Eq. (21)]. The total flux at the wall does not include induced wall currents in this quasi-DC case, but does include a constant term Φ_0 representing the static external n=1 field [Eq. (22)]. The model for the plasma response remains the same [Eq. (23)], but we now consider the stable case where $-1 < \gamma_0 < 0$ (in this model, $\gamma_0 = -1$ represents the case without plasma).

In DIII–D operation, the reference level for feedback control is typically determined after the coil currents and plasma currents are established, but before the plasma beta is raised. Therefore, to first approximation, the sensors do not detect static n=1 error fields (due to coil misalignments, for example) but do detect the plasma's response to these error fields as beta increases. In this quasi-DC case we neglect induced wall currents in Eqs (6-10), and the sensor signals become

Idealized Mode Detection or B_p sensor $\quad \Phi_S = \Phi_P \quad ,$ (24)

Smart Shell B_r Sensor $\quad \Phi_S = \Phi_P + \Phi_C \quad .$ (25)

The poloidal field sensor detects only the plasma perturbation and thus is equivalent to the idealized sensor. The smart shell B_r sensor detects flux from the plasma and the control coil, but

not the static n=1 error field. Substituting these sensor definitions into the model of Eqs. (21–23) we find:

Idealized Mode Detection or B_p sensor $\quad \Phi_P = 0$, (26)

Smart Shell B_r Sensor $\quad \Phi_P = \Phi_0 (1+\gamma_0)$. (27)

For comparison, the case without feedback ($\Phi_S \neq 0$, $\Phi_C = 0$) would give

No feedback $\quad \Phi_P = \Phi_0 (1+\gamma_0) / (-\gamma_0)$. (28)

The no-feedback case [Eq. (28)] shows the expected resonant behavior, with the plasma response becoming infinite at marginal stability ($\gamma_0 = 0$). The B_p sensor with a perfect feedback system reduces the plasma perturbation to zero [Eq. (26)]. However, the smart shell B_r sensor is only capable of reducing the plasma perturbation to a level comparable to the external error field [Eq. (27)], which could still lead to significant drag on the rotation.

In principle, the AC compensated B_r sensor [Eq. (9)] could be equivalent to the B_p sensor for suppression of resonant field amplification, despite its poorer predicted performance against unstable modes. This comparison has not yet been explored experimentally. The DC compensated B_r sensor [Eq. (8)] is limited to gains less than unity, and would be no more effective than the smart shell system.

6. CONCLUSIONS

Internal radial field and poloidal field sensors have been installed in DIII–D as input to the resistive wall mode feedback control system. DIII–D experimental results show good qualitative agreement with the predictions of simple analytic models and more realistic numerical models: internal radial field sensors provide a modest improvement over radial field sensors outside the wall, and internal poloidal field sensors provide a significant advantage over both sets of radial field sensors. The improvement with poloidal field sensors is predicted and observed for both direct feedback stabilization of the RWM and suppression of resonant field amplification.

REFERENCES

[1] A. Garofalo, et al., Phys. Plasmas **9**, (2002) 1997.

[2] Y.Q. Liu, et al., Phys. Plasmas **7**, (2000) 3681.

[3] A. Bondeson, et al., Nucl. Fusion **41**, (2001) 455.

[4] Y. Liu and A. Bondeson, Plasma Phys. Control. Fusion **44**, (2002) L21.

[5] A. Bondeson, et al, Nucl. Fusion **42**, (2002) 768.

[6] A. Bondeson, et al., Phys. Plasmas **9**, (2002) 2044.

[7] J. Bialek, et al., Phys. Plasmas **8**, (2001) 2170.

[8] M. Okabayashi, et al., Phys. Plasmas **8**, (2001) 2071.

[9] A.M. Garofalo, T.H. Jensen and E.J. Strait, "Semiquantitative Analysis of Feedback Systems for Resistive Wall Modes," to be published in Phys. Plasmas (2002).

[10] M. Okabayashi, et al., "Stabilization of the Resistive Wall Mode in DIII–D by Plasma Rotation and Magnetic Feedback", submitted to Plasma Phys. Control. Fusion (2002).

[11] M. Okabayashi, et al., "Resistive Wall Mode Control on the DIII–D Device," General Atomics Report GA-A 23892, submitted to Journal of Plasma and Fusion Research (2002).

[12] L.C. Johnson, et al., in Proc. 28th EPS Conference on Contr. Fusion and Plasma Phys. (Funchal, 2001) Europhysics Conference Abstracts, Vol. 25A (2001) 1361.

[13] A.H. Boozer, Phys. Rev. Lett. **88** (2001) 5059.